PLOS ONE

RESEARCH ARTICLE

Morin Flavonoid Adsorbed on Mesoporous Silica, a Novel Antioxidant Nanomaterial

Francisco Arriagada[1], Olosmira Correa[1], Germán Günther[2], Santi Nonell[3], Francisco Mura[4], Claudio Olea-Azar[4], Javier Morales[1]*

1 Departamento de Ciencias y Tecnología Farmacéuticas, Facultad de Ciencias Químicas y Farmacéuticas, Universidad de Chile, Sergio Livingstone, 1007, Independencia, Santiago, Chile, **2** Departamento de Química Orgánica y Fisicoquímica, Facultad de Ciencias Químicas y Farmacéuticas, Universidad de Chile, Sergio Livingstone, 1007, Independencia, Santiago, Chile, **3** Institut Químic de Sarriá (IQS), University Ramón Llull, Via Augusta, 390, 08017, Barcelona, Spain, **4** Departamento de Química Inorgánica y Analítica, Facultad de Ciencias Químicas y Farmacéuticas, Universidad de Chile, Sergio Livingstone, 1007, Independencia, Santiago, Chile

* javiermv@ciq.uchile.cl

Citation: Arriagada F, Correa O, Günther G, Nonell S, Mura F, Olea-Azar C, et al. (2016) Morin Flavonoid Adsorbed on Mesoporous Silica, a Novel Antioxidant Nanomaterial. PLoS ONE 11(11): e0164507. doi:10.1371/journal.pone.0164507

Editor: Bing Xu, Brandeis University, UNITED STATES

Received: August 6, 2016

Accepted: September 26, 2016

Published: November 3, 2016

Data Availability Statement: Data can be found on Figshare: //figshare.com/articles/PONE-D-16-31535R1_DATA_SET_pptx/3978069.

Funding: This work was supported by FONDECYT (grant 1160757 to JM), CONICYT (grant 21160932 to FA) and CONICYT (grant 21120376 to FM).

Competing Interests: The authors have declared that no competing interests exist.

Abstract

Morin (2´,3, 4´,5,7-pentahydroxyflavone) is a flavonoid with several beneficial health effects. However, its poor water solubility and it sensitivity to several environmental factors avoid its use in applications like pharmaceutical and cosmetic. In this work, we synthetized morin-modified mesoporous silica nanoparticles (AMSNPs-MOR) as useful material to be used as potential nanoantioxidant. To achieve this, we characterized its adsorption kinetics, isotherm and the antioxidant capacity as hydroxyl radical (HO•) scavenger and singlet oxygen ($^1O_2$) quencher. The experimental data could be well fitted with Langmuir, Freundlich and Temkin isotherm models, besides the pseudo-second order kinetics model. The total quenching rate constant obtained for singlet oxygen deactivation by AMSNPs-MOR was one order of magnitude lower than the morin rate constant reported previously in neat solvents and lipid membranes. The AMSNPs-MOR have good antioxidant properties by itself and exhibit a synergic effect with morin on the antioxidant property against hydroxyl radical. This effect, in the range of concentrations studied, was increased when the amount of morin adsorbed increased.

1. Introduction

The emerging discipline of nanomaterials intends to apply physical principles common in materials science to challenges in areas such as drug delivery, structure and properties of powders and manufacturing and processing of particle systems for use in novel formulations [1–3]. Nanoparticles (NPs) have been used to incorporate (by occlusion [4], non-covalent adsorption [5] and covalent attachment [6]) different molecules (drugs [7], photosensitizers [8], biomolecules [9], antioxidants [10], and others [11]) and to release them in a controlled way. Nanoparticles have frequently been prepared using biomolecules (proteins [12], lipids [13, 14]), polymers [15, 16], metals [17, 18] and oxides such as silica [19].

Silica (SiO_2) is an attractive material for chemistry, medicine and pharmaceutical sciences because it is optically transparent, chemically inert, mechanically stable, fairly biocompatible, and

its synthesis is relatively easy [20, 21]. Additionally, surface functionalization of silica is well-established using a wide variety of coating procedures [22–24]. Thereby, mesoporous SiO_2 nanoparticles (MSNPs) coated with amino groups (AMSNPs) have been used for adsorption, stabilization and separation of carboxylic and phenolic compounds by hydrogen bond interactions [25, 26].

Morin (2′,3,4′,5,7-pentahydroxyflavone) (Fig 1) is a phenolic compound present in vegetables and plants [27]. Several beneficial effects have been described, including anticancer [28], anti-inflammatory [29] and cardiovascular protective effects [30–32]. Moreover, morin (MOR) has shown interesting protective effects against UV-B radiation [33, 34], therefore its incorporation in topical formulation can be beneficial for skin health. However, its technological application (pharmaceutical and cosmetic formulations) is limited because this polyphenolic compound is sensitive to several environmental factors such as light, oxygen and pH among others [35].

Some studies have shown that morin is an efficient antioxidant owing to its ability to scavenge free radicals [36, 37] and quench singlet oxygen ($^1O_2$) [38–40]. The antioxidant capacity of polyphenols has been determined in different nanoparticles by evaluating the scavenging of 2,2-diphenyl-1-picrylhydrazyl (DPPH) free radical [41, 42]. Despite the potential benefits of using SNPs as vehicles for antioxidants, there are no studies describing effects of silica-bound morin or other flavonoids on $^1O_2$ and hydroxyl radical (HO•) scavenging.

In this work, we synthetized morin-modified silica nanoparticles (AMSNPs-MOR) as useful antioxidant nanomaterial. Specifically, we characterized morin adsorption kinetics and isotherm onto AMSNPs and the antioxidant capacity of the resulting nanostructured material as HO• scavenger and $^1O_2$ quencher.

2. Materials and Methods

2.1. Materials

Morin dihydrate was purchased from Merck. All chemicals (cetyltrimethylammonium bromide (CTAB) (Aldrich), ammonium hydroxide (NH_4OH) (J.T. Baker), hydrochloric fuming acid 37% (Merck), tetraethylortho-silicate (TEOS), 3-aminopropyltriethoxysilane (APTES)

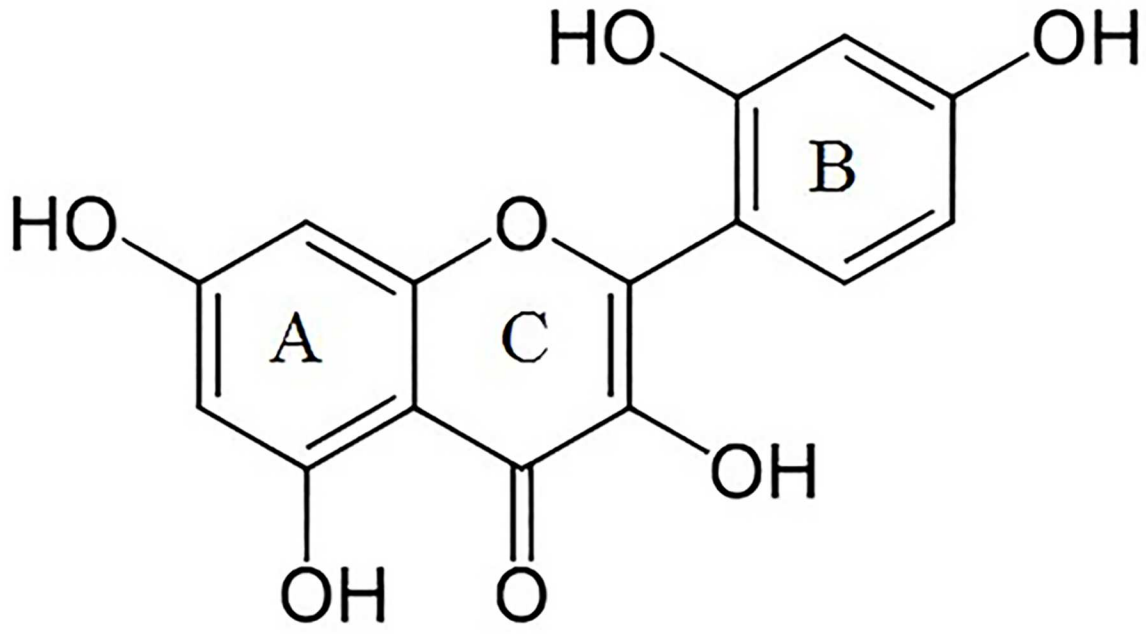

Fig 1. Chemical structure of morin.

doi:10.1371/journal.pone.0164507.g001

(Aldrich), glycerin (Merck), polyoxyethylene sorbitan monooleate (polysorbate) 80 (Aldrich), sodium lauryl sulfate (Winkler) and chloride benzalkonium (reagent grade)) were used as received without any further purification.

Rose Bengal (RB) and 5,5-dimethylpyrroline N-oxide (DMPO) were purchased from Sigma-Aldrich and hydrogen peroxide 30% v/v was obtained from Merck.

All solvents used were reagent grade or HPLC quality. Water was purified and deionized using a Milli-Q system.

2.2. Methods

2.2.1. Synthesis and surface modification of mesoporous silica nanoparticles. Mesoporous silica nanoparticles (MSNPs) were synthesized using a modified Stöber method [43] by slowly adding 7.2 mL tetraethyl orthosilicate (TEOS) to a mixture of 120 mL ethanol, 44 mL deionized water, 80 mg CTAB and 7.2 mL ammonia solution in a thermostated round bottom flask at 60°C under stirring.; then stirring was stopped, allowing the reaction to proceed for 2 h. The resulting dispersion was washed with several portions of ethanol followed by centrifugation and resuspension of the MSNPs and then 8 mL of HCl 37% were added and kept under stirring at 60°C for 12 h. The resulting suspension was washed again with several portions of ethanol followed by centrifugation and resuspension. The final MSNPs obtained were re-suspended in ethanol.

Aminopropyl-modified silica nanoparticles (AMSNPs) were prepared by treating MSNPs with (3-aminopropyl) triethoxysilane (APTES). MSNPs were suspended in 200 mL toluene and 0.8 mL of APTES were added at room temperature. The mixture was then heated to reflux for 24 h and allowed to cool. The nanoparticles were washed and centrifuged several times with portions of toluene, toluene: ethanol and ethanol and stored re-suspended in ethanol.

2.2.2. Morin adsorption. Adsorption experiments were carried out in batch mode in triplicate to obtain the equilibrium and kinetic data [44, 45]. Preliminary experiments were done to figure out the optimal conditions for batch adsorption. A morin stock solution of 2 mg mL^{-1} was prepared and different desired volumes were taken and added to 30 mL of AMSNPs suspension in a flask. After addition of morin aliquot, the suspensions were stirred at 100 rpm until adsorption equilibrium was reached and subsequently centrifuged to 8000 rpm for 20 min to obtain suitable aliquots for analysis of residual morin concentration by an HPLC method previously developed and validated [46]. Thus, AMSNPs-MOR or just NP-MOR were obtained.

2.2.3. Adsorption isotherms. Isotherm determination experiments were carried out by adding a fixed amount of morin solution (0.514 mg MOR /mL EtOH) to varying amounts of AMSNPs (15 mg—100 mg) in a volumetric flask (25 mL) to obtain a final morin concentration of $1x10^{-4}$ M; then the flask contents were stirred until adsorption equilibrium was reached. The amount of morin adsorbed at equilibrium onto the nanoparticles surface was calculated from the following equation [47]:

$$q_e = \frac{(C_0 - C_e)V}{m} \quad \text{Eq 1}$$

Where q_e is the amount of morin adsorbed per unit amount of AMSNPs nanoparticle at equilibrium (given in mg g^{-1}), C_0 and C_e are the morin concentrations in solution before and after adsorption, respectively (mg L^{-1}), V is the bulk volume of the medium (L) and m is the mass of nanoparticles (g).

2.2.4. Adsorption kinetics. The kinetics of morin adsorption onto AMSNPs was assessed by adding an aliquot of morin solution (2 mg mL^{-1}) to nanoparticle suspensions (1.2 g mL^{-1}).

The suspension was kept at 25°C under stirring. At several time intervals, samples were collected, centrifuged, and the concentration of morin in the supernatant was determined by HPLC. The amount of morin adsorbed per unit amount of nanoparticle after each time interval q_t (mg g^{-1}), was calculated by the following equation:

$$q_t = \frac{(C_0 - C_t)V}{m} \quad \text{Eq 2}$$

Where C_0 is the initial concentration of morin (mg L^{-1}) and C_t is the concentration at time "t" (mg L^{-1}), V and m having the same meaning as above.

2.2.5. Nanoparticle characterization. The average particle size, polydispersity index and Zeta potential of MSNPs, AMSNPs and AMSNPs-MOR were analyzed using a Malvern Zetasizer Nano ZS90 (Malvern, UK). The samples were diluted with ethanol and different pH buffers. Morphological characterization was based on scanning electron microscopy (SEM) FEI™, inspect F50 model, where the samples were placed on a silicon wafer grid and then coated with gold. Fourier transform infrared (FT-IR) spectra were obtained on an Interspec 200-X FT-IR spectrometer with 4 cm^{-1} resolution in the wavenumber range of 4000–400 cm^{-1} and 16 scans were taken with the average from each spectrum.

2.2.6. Morin removal from nanoparticles. In order to evaluate the removal of morin from the nanoparticles-morin caused by different components frequently used in commercial pharmaceutical and cosmetic formulations, such as glycerin (5% and 10%), polysorbate 80 (0.5% to 5%), sodium lauryl sulfate (0.05% to 0.5%), and benzalkonium chloride (0.01% to 0.1%), AMSNPs with adsorbed morin (AMSNPs-MOR or just NP-MOR) were suspended in 10 mL of each of the above mentioned solutions and kept in contact under gentle stirring until equilibrium was reached; then, the suspension was centrifuged and the concentration of morin in solution was quantified by HPLC [46].

2.2.7. Singlet oxygen quenching. The total quenching rate constant (k_T) for the deactivation of $^1O_2$ by AMSNPs-MOR was determined in D_2O suspensions by monitoring the time-resolved phosphorescence of $^1O_2$ following laser excitation of Rose Bengal (RB) electrostatically adsorbed onto AMSNPs (NP-RB).

Time-resolved $^1O_2$ near-infrared phosphorescence was measured by means of a PicoQuant FluoTime 300 fluorescence lifetime spectrometer. A PLS 575 LED-head was employed as the pulsed light source, in burst mode. Luminescence of singlet oxygen was monitored at 1270 nm using a Hamamatsu NIR-PMT detector (H10330-45) and analyzed with PicoQuant's Fluofit software.

2.2.8. Hydroxyl radical scavenging. The antioxidant capacity of AMSNPs-MOR against the hydroxyl radical (HO•) was assessed by spin-trapping using DMPO [48]. HO• was generated by photolysis of hydrogen peroxide using a UV-Vis-NIR light source model DH-2000-BAL purchased from Ocean Optics. Solutions of DMPO (200 mM) and of H_2O_2 (10% v/v) were prepared in Milli Q water. Morin was dissolved in a solution of glycerin 10% v/v with a small quantity of ethanol as co-solvent (0.2% of the final volume) to a final concentration of 0.11 mM. The control solution was prepared with DMPO 200 mM (50 μL), hydrogen peroxide 10% (50 μL) and glycerin 10% (50 μL). Due to the low adsorption efficiency (11 mg g^{-1}), the experimental concentration range achievable is limited and two concentrations of morin were selected (18 and 36 μM). The samples were prepared replacing the glycerin volume by a morin solution 0.11 mM (solution 1), AMSNPs solution 6800 mg L^{-1} (solution 2) and AMSNPs-MOR solution 0.11 mM (solution 3). In order to evaluate the presence of photolytic degradation paths (in absence of hydroxyl radical), an assay with morin was performed, observing the formation of a DMPO-HO• adduct in a small quantity (10% of the signals in the control spectrum), which was discounted on the intensity of the signals in all the measurements.

EPR spectra were recorded at the X band (9.81GHz) using a Bruker ECS106 spectrometer with a rectangular cavity and 50 kHz field modulation. Spectrometer conditions were: microwave frequency 9.81 GHz, microwave power 20 mW, modulation amplitude 0.91 G, receiver gain 59 dB, time constant 81.92 ms and conversion time 40.96 ms [49]. Each spectrum was obtained after 10 scans.

The antioxidant capacity was considered as directly proportional to the decrease in the area of the signal in comparison to a control spectrum, which did not contain any antioxidant.

$$Antioxidant\ capacity = \frac{A_{CONTROL} - A_{SAMPLE}}{A_{CONTROL}} \times 100 \quad \text{Eq 3}$$

Where $A_{CONTROL}$ is the area under a peak in the control spectrum, A_{SAMPLE} is the area under a peak in the spectra which an antioxidant (morin, AMSNPs or AMSNPs-MOR) is present.

2.3. Statistical analysis

Data are presented as mean ± SD of *n* independent experiments. Statistical analysis was performed using a R^2 parameter, Chi-Square test or one-way ANOVA and comparisons between groups were performed by Tukey`s multiple comparison test. $p < 0.05$ was considered significant.

3. Results and Discussion

3.1. Characterization of NPs

The changes in size were observed in the synthesis and upon addition of morin to 100 mg of AMSNPs, showing that morin was incorporated onto silica nanoparticles. The mean particle size of MSNPs, AMSNPs and AMSNPs-MOR obtained by Dynamic Light Scattering determinations were 105, 125 and 155 nm, respectively (values consistent with SEM images). Polydispersity indices ranged from 0.02 to 0.17 revealing high size homogeneity of these NPs. Previously, the mean pore size of MSNSPs and AMSNPs determined by TEM was about 3 nm (data not shown), similar pore size has been reported in other works [50–52]

A SEM image in Fig 2 shows the morphology of the AMSNPs-MOR. All NPs observed in SEM images were of similar size, showing a monodisperse sample.

Table 1 shows the results of zeta potential measurements for AMSNPs and AMSNPs-MOR (2 mg MOR / 100 mg NP) dispersed in solutions at pH 1, 3, 7 and 9. At pH 1 and 3 morin adsorbed on the nanoparticles does not change their positive Zeta potential value, possibly due to molar ratio between OH of morin structure and NH_2 of NP is not equivalent, therefore the effect of this flavonoid on the surface potential is not relevant. Moreover, at pH 7 and pH 9, morin is ionized (phenolate form), changing the nanoparticle surface potential (negative). The ionization of hydroxyl groups of flavonoids is highly dependent on their position, pK_a and the medium pH. At pH 7, only the hydroxyl located at position 2´ of the morin's B ring is ionized [53].

FTIR spectra were recorded in the range of 4000–400 cm^{-1}. The spectrum of morin (Fig 3A and 3B) reveals a band at 1653 cm^{-1} due to (C = O) stretching vibration, the (C-OH) deformation vibrations are observed at 1351 cm^{-1} and 1307 cm^{-1}. The peaks at 1202 cm^{-1} and 1172 cm^{-1} corresponding to the (C-OH) stretching and the band located at 1245 cm^{-1} are attributed to the (C-O-C) bending. The MSNPs spectrum in the Fig 3B showed a broad band (1200–1000 cm^{-1}) corresponding to the asymmetric vibration of group (Si-O-Si). Additionally, the bands at 940 cm^{-1} and 795 cm^{-1} are related to asymmetric vibration of Si-

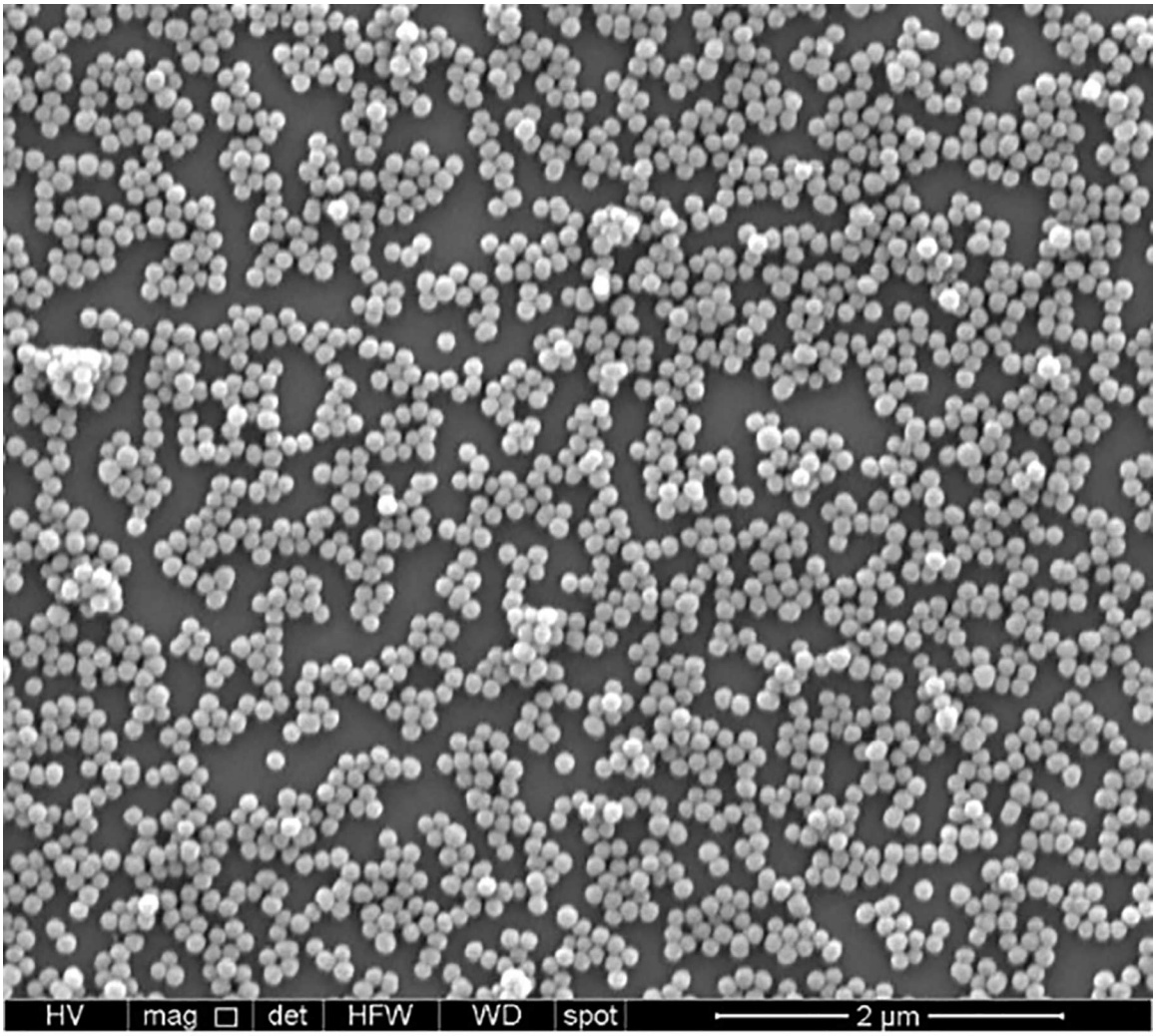

Fig 2. SEM micrograph of AMSNPs-MOR.

doi:10.1371/journal.pone.0164507.g002

OH and symmetric vibration of Si-O, respectively. Fig 3A showed a very characteristic absorption band at 3300 cm^{-1} assigned to O-H stretching in H-bonded water, also supported by the presence of 1630 cm^{-1} band due to scissor bending of molecular water. Moreover, the presence of the bands at 2985 cm^{-1} (CH_3) and 2935 cm^{-1} (CH_2) is attributed to the presence of unreacted TEOS [54].

Fig 3 displayed the AMSNPs spectrum, which shows some changes when compared with MSNPs spectrum; the band corresponding to O-H stretching (3300 cm^{-1}) of molecular water and the band of asymmetric vibration of Si-OH (940 cm^{-1}) decreased their intensity, besides bands at 2985 cm^{-1} and 2878 cm^{-1} slightly increased due to the vibration of (CH_2) group of the

Table 1. Zeta potential values of NPs dispersed in aqueous solutions at different pH.

Nanoparticles	Zeta potential (mVolts)			
	pH 1	pH 3	pH 7	pH 9
AMSNPs	+41.8	+27.6	-1.5	-5.2
AMSNPs-MOR	+44.7	+26.2	-9.5	-17.7

doi:10.1371/journal.pone.0164507.t001

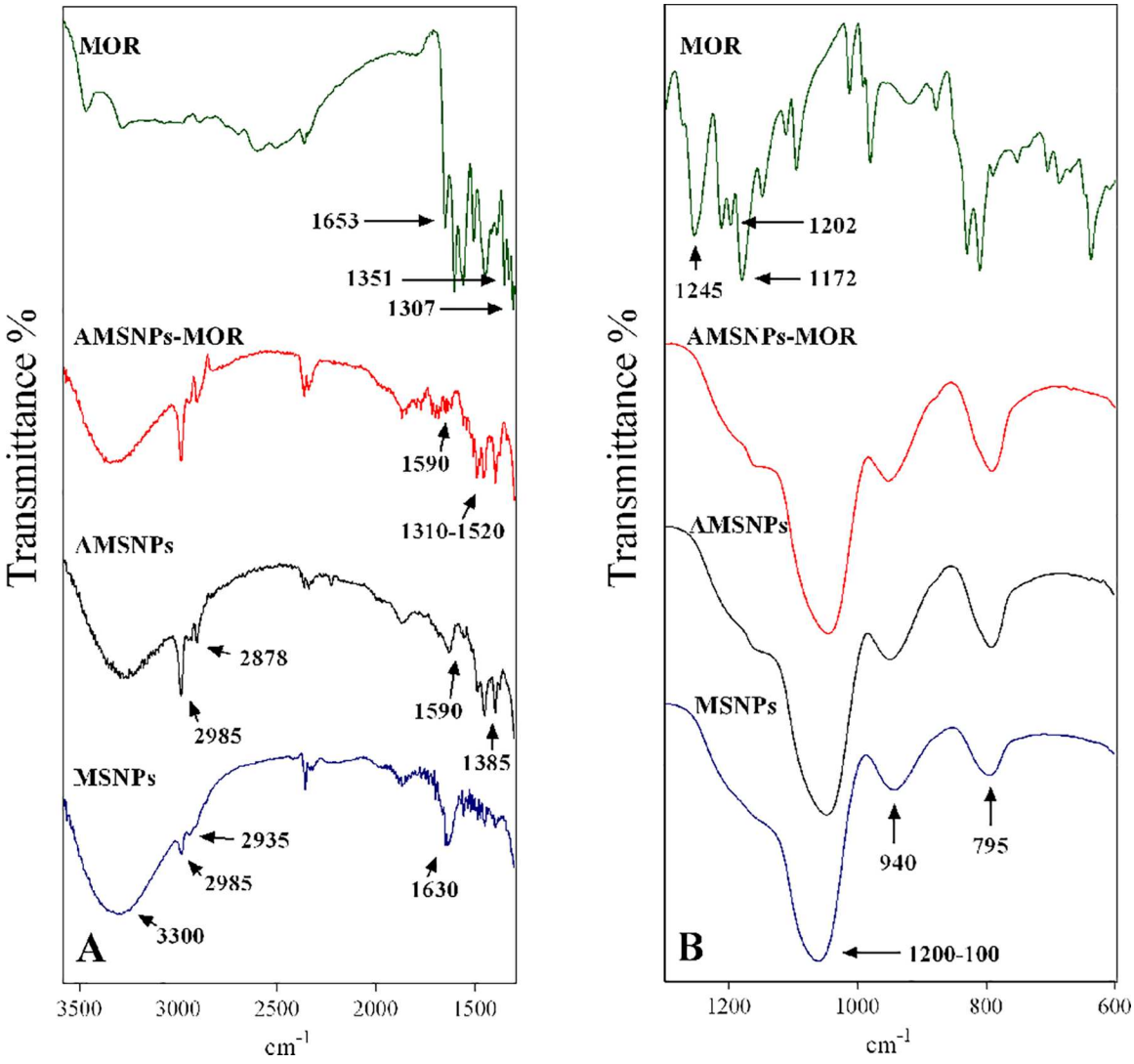

Fig 3. FTIR spectra. (A) MSNPs (blue), AMSNPs (black), AMSNPs-MOR (red) and morin (green) in the range of 3600–1300 cm^{-1} and (B) MSNPs (blue), AMSNPs (black), AMSNPs-MOR (red) and morin (green) in the range of 1299–600 cm^{-1}.

doi:10.1371/journal.pone.0164507.g003

propyl chain and a new band at 1385 cm^{-1}, corresponding to the Si-CH_2 bending mode was observed, suggesting the presence of the amino group of APTES molecule in the terminal position of the propyl chain; also a new band assigned to NH_2 asymmetric bending was observed at 1590 cm^{-1}. This implies that the concentration of Si-OH groups in the surface has decreased and the amount of NH_2 groups has increased, suggesting a successful APTES functionalization [55–58]. The IR spectrum of NP-MOR showed at least three significant differences in comparison with MSNPs and AMSNP spectra. First, in the region of 1310–1520 cm^{-1} some changes were observed due to superposition and/or shift of the bands corresponding to the C-C skeletal vibration of morin aromatic ring. Second, the band ascribed to the NH_2 asymmetric bending diminished considerably, these findings suggest that morin was successfully incorporated onto silica nanoparticles through the interaction with NH_2 group of APTES. Finally, the bands centered at 3300 cm^{-1} increased their intensity, because of the morin–OH groups, present now in nanoparticles surface, observation in agreement with other authors. These results suggest that

interaction between nanoparticles and morin, involves NH_2 group of APTES and OH group of A or C ring of morin. In fact, Vergara-Castañeda et al. [59] reported the linking of quercetin onto silica nanoparticles, they state that quercetin conjugation in the NPs involves a covalent-like bond through amide groups of APTES-NPs with OH and/or C = O groups of quercetin. Nevertheless, more tests are necessary to unravel the exact way by which incorporation takes place. On the other hand, different antioxidant measurements allow us to elucidate the possible point of linkage, considering the different antioxidant capacity of morin functionalities.

3.2. Adsorption properties

It is well known that the adsorption capacity of a surface is frequently determined by the degree of compatibility between adsorbent and adsorbate [60]. This is important because the interaction between adsorbate and adsorbent is fundamental for the design of the adsorption system [61]. For batch adsorption experiments, the morin concentration was 5.9 x 10^{-3} M. Fig 4A shows the data obtained (in triplicate) of the adsorbed amount of morin onto nanoparticles versus the initial amount of morin. The maximum adsorption obtained was 11 mg g^{-1}. The adsorbed amount increases when the initial amount of morin increases, reaching saturation at initial morin values above 8–10 mg.

Higher adsorption values were obtained compared with other reports about flavonoid adsorption onto silica nanoparticles [42]. This must be due to surface functionalization with

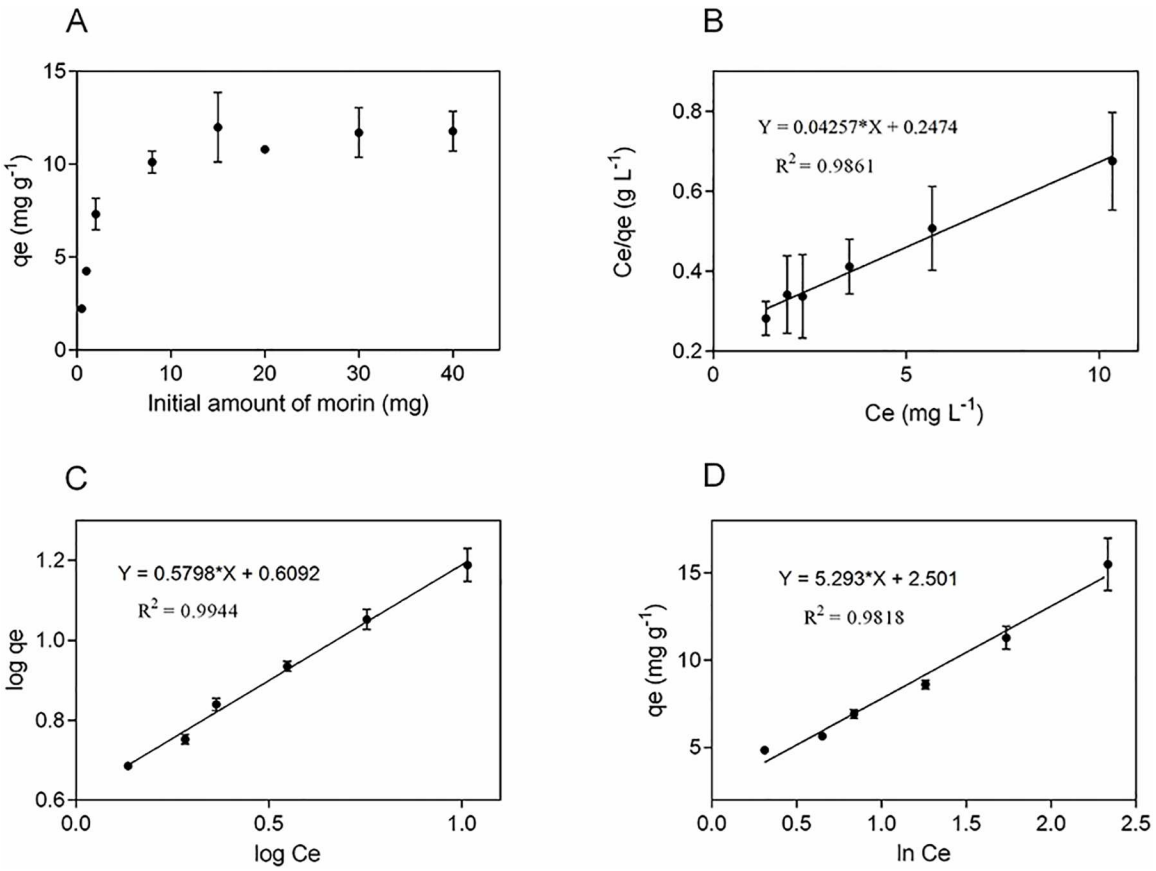

Fig 4. Morin adsorption onto silica nanoparticles. (A) Adsorbed amount of morin as a function of different initial amount of morin; linear fit of experimental data obtained using (B) Langmuir (C) Freundlich and (D) Temkin isotherm models at 25˚C. Values are the mean of n = 3 (mean± SD).

doi:10.1371/journal.pone.0164507.g004

APTES, as reported by Berlier et al. [62] using rutin; these authors hypothesized that it is possible that the aminopropyl chains play an important role in the van der Waals interaction with the quercetin aglycone. It is clear that the type of functionalization plays a pivotal role in the adsorption capacity; it also is affected by the physicochemical and structural characteristics of the adsorbed molecule. Previous experiments in our laboratory showed a decrease in the adsorption of quercetin on silica nanoparticles upon functionalization with APTES, around half of that obtained with morin (data not shown).

3.3. Adsorption isotherms

The function that expresses the magnitude of the retention and behavior of a molecule on a solid surface once the equilibrium of adsorption/desorption phenomena have been reached, it can be described from the relationship between the remaining concentration of a molecule with the concentration or amount of the same compound retention on the surface at constant temperature, this relationship is commonly known like as Adsorption Isotherm [44, 63].

The Langmuir [64, 65], Freundlich [66] and Temkin [67] isotherm models are often used to describe the adsorption equilibrium and provide an approach to elucidate the adsorption mechanism, the surface properties and also the degree of affinity of the adsorbent for the adsorbate. Langmuir model assumes a monolayer adsorption, this suggests that the adsorption occurs at a finite number of localized sites, with no lateral interaction and steric hindrance between the adsorbed molecules; according to this, exists a maximum adsorption when a saturated monolayer of molecules is produced on the surface. On the other hand, Freundlich is an empiric model that describes the non-ideal and reversible multilayer adsorption, applicable to heterogeneous surfaces with non-uniform distribution of adsorption heat and intensity of affinity over the surface. Temkin model considers the effects of some indirect adsorbate-adsorbate interactions on adsorption isotherms and suggests these interactions would decrease linearly the heat of adsorption with the increase of coverage.

In order to determine the maximum adsorption capacity of the nanoparticles and to better describe the relationship between adsorbent and adsorbate at equilibrium conditions, we analyzed our data according to the linearized forms of Langmuir, Freundlich and Temkin adsorption isotherms, which correspond to the following equations:

$$\frac{C}{q_e} = \frac{1}{Q_m b} + \frac{1}{Q_m} c \qquad \text{Eq 4}$$

$$\log(q_e) = \log K_f + \frac{1}{n} \log C \qquad \text{Eq 5}$$

$$q_e = B \ln A + B \ln C_e \qquad \text{Eq 6}$$

Where q_e is the equilibrium concentration of morin on the solid surface phase (mg g^{-1}), C is the concentration of morin in solution (mg L^{-1}), Q_m is the maximum monolayer uptake by the nanoparticles (mg g^{-1}), and b is the Langmuir constant for the equilibrium adsorbate-adsorbent (L mg^{-1}). K_f is the Freundlich coefficient ((mg g^{-1})(L $mg^{-1})^{1/n}$), where n is the Freundlich constant (index of adsorption intensity or surface heterogeneity) which denotes a favored adsorption if the value lies between 1 and 10 (chemisorption process is favored and the surface is more heterogeneous when slope, $1/n$, value approaches zero) [66]. A is the Temkin isotherm constant (L·mg^{-1}), B is a constant defined as $B = \frac{RT}{b_T}$, where T is the absolute temperature in Kelvin, R is the universal gas constant (8.3143 J mol^{-1} K^{-1}) and b_T is a constant related to the heat of adsorption.

The experimental data could be well fitted with Langmuir, Freundlich and Temkin isotherm models (Fig 4), showing a high coefficient of determination for three models ($R^2_{Freundlich}$ = 0.9944; $R^2_{Langmuir}$ = 0.9861; R^2_{Temkin} = 0.9818).

While the three models seem to appropriately describe the data, the high correlation of the data with the Freundlich model suggests that it is most suitable to fit. The above results suggest that morin adsorption onto the surface of the nanoparticles is not restricted to the formation of a monolayer but follows a multilayer adsorption, with non-uniform distribution of adsorption heat and affinities over the heterogeneous surface [44, 67]. On the other hand, the coefficients of determination coefficients for the Langmuir and Temkin isotherm models are statistically significant, indicating that the adsorption process also involves the formation of a monolayer of morin. This could be explained because the adsorption-desorption equilibrium can be a complex process controlled by more than one mechanism, where dimer formation and possible self-assembly of morin in piled up form [68], could generate multilayers at the surface, involving electrostatic forces. The parameter *n* equal to 1.72, higher than 1, indicates a favorable adsorption process.

Based on the non-linear Chi-square statistical analysis [69], we found that the data fit better to the Langmuir model although the R^2 is smaller in comparison to the Freundlich model, these results suggest a better concordance with the experimental data, in fact, the maximum monolayer uptake value (23.5 mg g^{-1}) was calculated from the equation of the linearized Langmuir isotherm, this value was consistent with the experimental value of the maximum adsorption, determined from the plateau in Fig 4.

Furthermore, the feasibility of the adsorption can be elucidated from the dimensionless constant, commonly known as separation factor (R_L) [70], and can be represented as:

$$R_L = \frac{1}{1 + bC_0} \quad \text{Eq 7}$$

Where *b* is the Langmuir constant (L mg^{-1}) and C_0 is the initial concentration of morin (mg L^{-1}). R_L values indicate the nature of the adsorption for an unfavorable reaction ($R_L > 1$), linear case ($R_L = 1$), favorable process ($0 < R_L < 1$) and irreversible case ($R_L = 0$). The R_L values were 0.26–0.009 at 25°C, suggesting that the adsorption process is favorable. The values of the different parameters obtained from the linearized isotherm models are summarized in Table 2.

Table 2. Adsorption isotherms parameters of morin onto AMSNPs.

Isotherm	Equation	Parameters
Langmuir	$(C/q_e) = (1/(Q_m b)) + (1/Q_m) C$	Q_m (mg g^{-1}) = 23.5
		b (L mg^{-1}) = 0.172
		R^2 = 0.9861
		R_L = 0.25–0.009
		X^2 = 34.5
Freundlich	$\log(q_e) = \log K_f + (1/n) \log C$	K_f ((mg/g)(L/mg)$^{1/n}$) = 4.1
		n = 1.72
		R^2 = 0.9944
		X^2 = 564.1
Temkin	$q_e = B \ln A + B \ln C_e$	B = 5.293
		A (L mg^{-1}) = 1.6
		R^2 = 0.9818
		X^2 = 69.1

doi:10.1371/journal.pone.0164507.t002

3.4. Adsorption kinetics

The study of adsorption kinetics is crucial because it can unravel both the adsorption and the desorption mechanisms [61]. The rate of adsorption may be determined by mechanisms such as chemical reaction, mass transfer, diffusion control or a combination of them [71]. Since adsorption is a time-dependent process, it is useful to determine its rate in order to evaluate or design the adsorbent [72].

Fig 5A shows the effect of contact time, maximum adsorption is reached after 10 h during a gradual adsorption process. After that, a second stage was observed leading to a final equilibrium state, possibly due to a decrease in the number of available adsorption sites, as well as to the decrease in the concentration of morin in solution phase.

Various kinetics models have been suggested to describe the adsorption process, and new derivation methods have been proposed to optimize established models to provide a better understanding of the various processes and to establish conditions that limit the use of each model; although results are debatable, valuable approaches are presented for the various theoretical viewpoints of the models [61, 73, 74]. Considering this, the kinetics of morin adsorption onto the nanoparticle surface was analyzed using three different kinetic models: the pseudo-

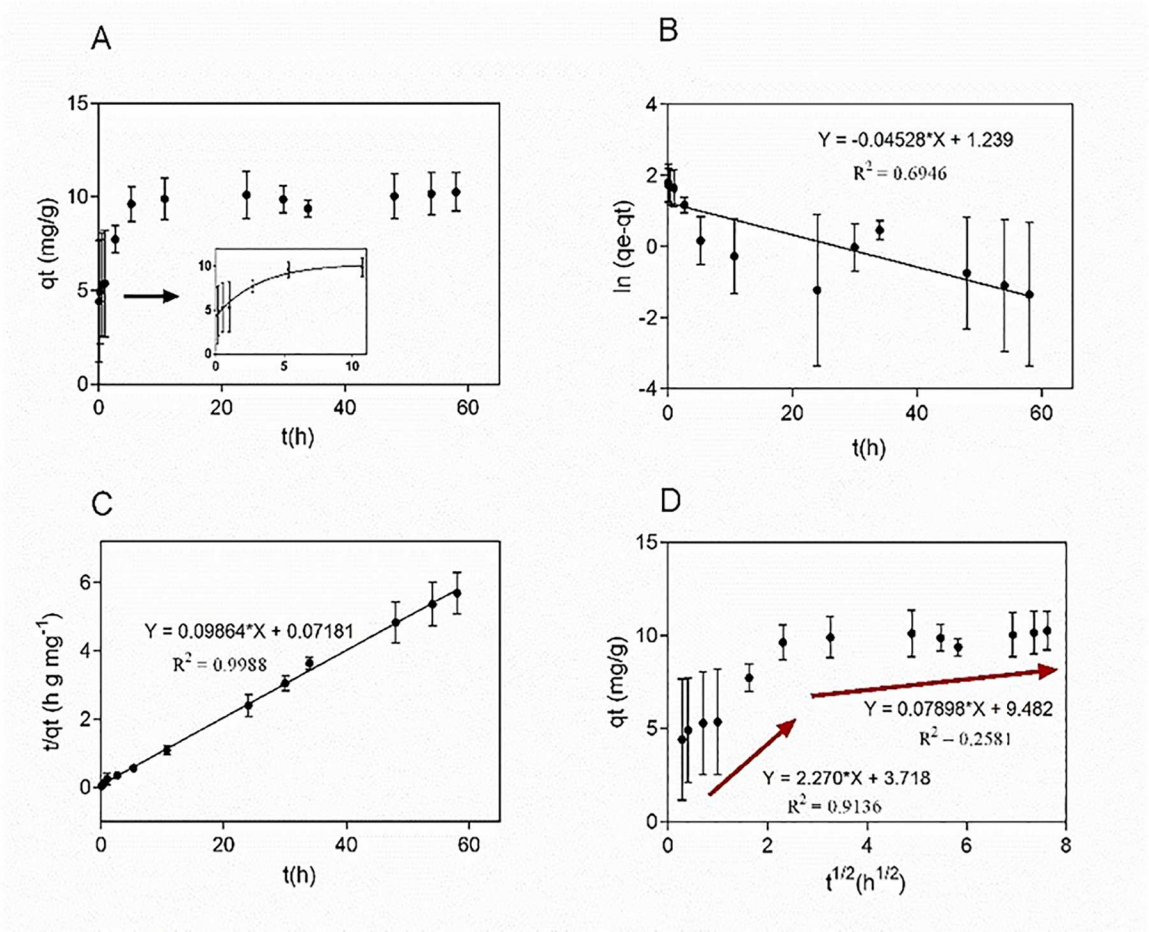

Fig 5. Adsorption kinetics of morin onto AMSNPs. (A) Effect of contact time; (B) linear fit of experimental data obtained using pseudo-first order model, (C) pseudo-second order model and (D) intra-particle diffusion model. Values are the mean of n = 3 (mean± SD).

doi:10.1371/journal.pone.0164507.g005

first-order proposed first by Lagergren (Eq 8) [75], the pseudo-second-order models of Ho and McKay [76] (Eq 9) and Weber and Morris intra-particle diffusion model (Eq 10) [77]:

$$\ln(q_e - q_t) = \ln q_e - k_1 t \quad \text{Eq 8}$$

$$\frac{t}{q_t} = \frac{1}{k_2 q_e^{\,2}} + \frac{t}{q_e} \quad \text{Eq 9}$$

$$q_t = K_{id} t^{1/2} + I \quad \text{Eq 10}$$

Where q_e and q_t are the amount of adsorbed morin onto nanoparticle surface at equilibrium and at time t (mg g^{-1}), respectively; k_1 is the observed rate constant of the pseudo-first order model (h^{-1}) and k_2 is the observed rate constants of the pseudo-second-order model (g mg^{-1} h^{-1}). K_{id} is the intra-particle diffusion rate constant (g/mg $h^{1/2}$) and I is related with the thickness of the boundary layer.

Fig 5B and 5C show the linear fit to pseudo-first order and pseudo-second-order equation, respectively. k_1 was obtained from the slope of plot $\ln(q_e - q_t)$ versus t; k_2 was obtained from the intercept and slope of plot t/q_t versus t. The q_e value obtained with pseudo-first-order model is far from the experimentally found value, suggesting that the model, despite the good fit, does not describe the process, on the other hand, q_e value given by the pseudo-second-order treatment is much closer to that found experimentally. The values of R^2 suggest that the pseudo-second-order model is more suitable to predict the kinetic mechanism for the adsorption of morin onto silica nanoparticles in the present work.

The stages of adsorption process are studied thoroughly with Weber and Morris intraparticle diffusion model which is observed in Fig 5D. According to the Eq (10), if the plot gives a straight line, then the adsorption is controlled solely by the intraparticle diffusion, but the adsorption data present a multi-linear plot, a gradual adsorption following by the final equilibrium of the process, showing that there are more than one step involved in the adsorption process [78]. All results suggest a complex process where rate-limiting step of adsorption could be a chemisorption rather than an intra-particle diffusion only. Only a few studies involving adsorption of flavonoids onto silica nanoparticles for pharmaceutical and/or cosmetic purposes have been reported, and even less works depict the kinetic process of morin on such a pharmaceutical carrier. Other works about kinetic processes involving silica nanoparticles obtained similar results to those reported here, namely that the pseudo-second order model is more suitable to predict the behavior of different compounds adsorbed onto AMSNPs in that case [79–81]. The data obtained from Eqs 8 to 10 are summarized in Table 3.

Table 3. Adsorption kinetics parameters of morin onto AMSNPs.

Kinetics model	Equation	R^2	Parameters
Pseudo first-order	$\ln (q_e - q_t) = - 0.04528\ t + 1.239$	0.6946	$k_1 = 0.04528\ h^{-1}$
			$q_e = 3.45\ mg\ g^{-1}$
Pseudo second-order	$(t / q_t) = 0.09864\ t + 0.07181$	0.9988	$k_2 = 0.136\ g\ mg^{-1}h^{-1}$ $q_e = 10.14\ mg\ g^{-1}$
Intra-particle diffusion	$q_t = 2.27\ t^{1/2} + 3.718$	0.9136	$k_{id1} = 2.27\ mg\ g^{-1}h^{-1/2}$ $I_1 = 3.718\ mg\ g^{-1}$
	$q_t = 0.07898\ t^{1/2} + 9.482$	0.2581	$k_{id2} = 0.07898mg\ g^{-1}h^{-1/2}$ $I_2 = 9.482\ mg\ g^{-1}$

doi:10.1371/journal.pone.0164507.t003

3.5. Morin removal from nanoparticles

The morin removal from AMSNPs-MOR by effect of the presence of a polyol compound (glycerin) and anionic (sodium lauryl sulfate), cationic (benzalkonium chloride) and nonionic (polysorbate 80) surfactants was determined. Glycerin (GLY) solutions at 5% and 10% did not generate an effect on morin desorption (or removal). Polysorbate 80 solutions at 0.5%, 1%, 2% and 5% had a negligible effect on the removal. The removal generated by the solutions of sodium lauryl sulfate (SLS), did not exceed 5% at each concentration. Moreover, removal of morin by the benzalkonium chloride (BAC) was more significant, reaching average values of 44% of morin desorption in different tested concentrations, with a tendency to increase the desorption as the concentration increases (Fig 6).

These results can be explained because of the slight negative charge on the adsorbed morin which would interact with benzalkonium chloride (positively charged), causing increased desorption respect to the other components under study. It is interesting to mention that when the AMSNPs-MOR system is in contact with the different media studied, morin removal occurs only once, i.e. morin that is not removed is irreversibly adsorbed when the dispersion medium are those mentioned above. In order to force desorption of morin, we performed desorption experiments at 80°C; nevertheless, removal of morin was negligible and morin layer onto silica nanoparticles remained irreversibly adsorbed. This is consistent with the results discussed from isotherms and kinetic models. To discard the idea that the adsorption occurs in a priority way in the pore; we previously performed experiments with non-porous silica nanoparticles. Nevertheless, no significant differences in the adsorption compared with our porous

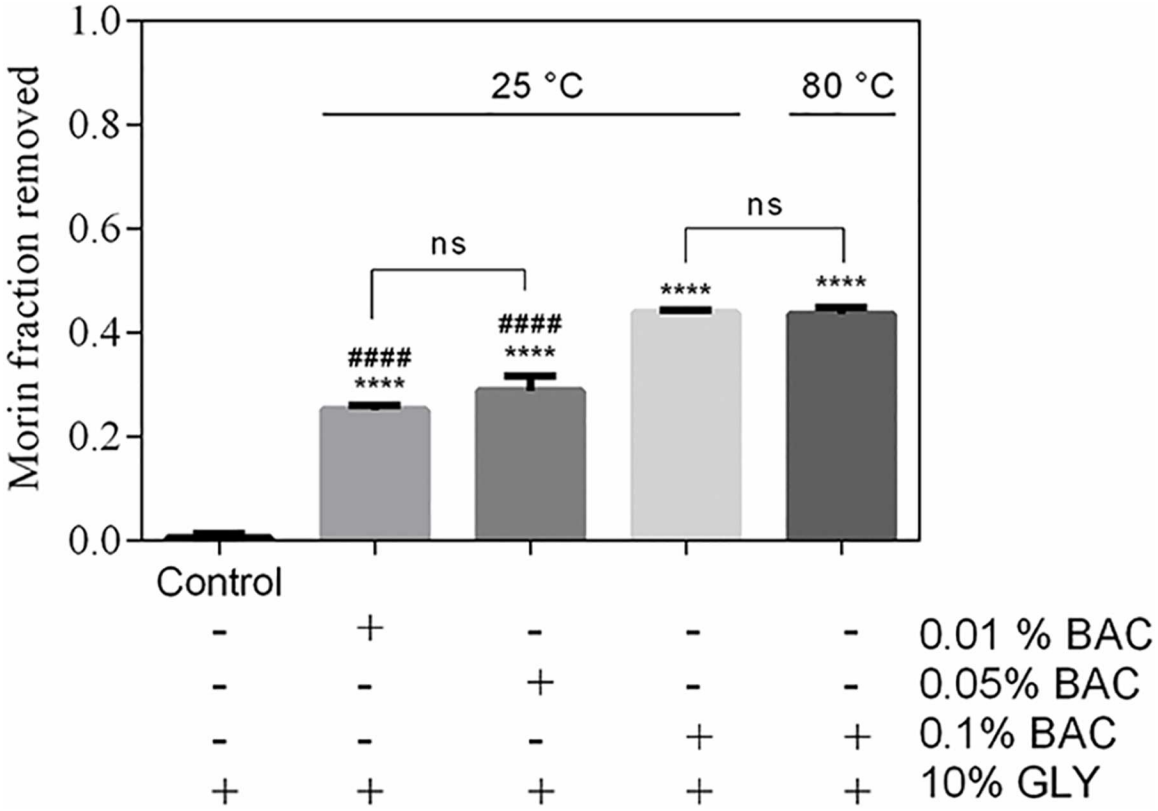

Fig 6. Removal of adsorbed morin by benzalkonium chloride (BAC). Values are the mean of n = 3 (mean± SD). ****p < 0.0001 vs. control, ####p < 0.0001 vs. 0.1% BAC at 25˚C or 0.01% BAC at 80˚C.

doi:10.1371/journal.pone.0164507.g006

silica nanoparticles were found. Thus, we hypothesized that removal of morin take place mainly on the nanoparticles surface.

Taken together, all results suggest a first layer of morin chemisorbed onto the nanoparticles; while external layers (association or self-assembly of morin in piled up form) are physisorbed and easily removed by typical components of pharmaceutical formulation e.g. benzalkonium chloride. Similar results has been mentioned by others authors, finding that the most probable route for flavonoid incorporation in the AMSNPs is by a conjugation based in covalent-like bonding [59].

3.6. Antioxidant capacity studies

3.6.1. Deactivation of singlet oxygen by AMSNPs-MOR. The singlet oxygen ($^1O_2$), an electronically excited species of oxygen, can be generated in biological systems usually by two different routes; by reactions known as "light reactions" and "dark reactions" produced by process like photo-excitation and chemi-excitation respectively [82]. In states of oxidative stress in the skin, various ROS are generated, including $^1O_2$, which can significantly alter different biomolecules like proteins, lipids and DNA, with undesirable consequences for health [83]. Therefore, deactivation of singlet oxygen, could help to avoid or reduce such kind of adverse effects.

The deactivation of singlet oxygen with a flavonoid or other quencher, involves physical quenching (deactivation) and/or chemical (reactivity) processes. The sum of the physical quenching (k_q) and chemical reaction (k_R) constants correspond to the total rate constant (k_T) [38, 39]. In this work, k_T values for the deactivation of singlet oxygen by AMSNPs-MOR dispersed in D_2O were obtained by measuring the first-order rate of singlet oxygen of luminescence decay in the presence and absence of morin (Eq 11).

$$\tau^{-1} = \tau_0^{-1} + k_T[MOR] \quad \text{Eq 11}$$

where τ^{-1} is singlet oxygen lifetime in presence of morin and $\tau_0{}^{-1}$is singlet oxygen lifetime in its absence ($\tau_0{}^{-1} = 1/k_d$). Values of k_T were calculated from slopes of τ^{-1} vs. [MOR] plots. Fig 7 shows the corresponding Stern-Volmer plot.

The obtained value of k_T (4.5×10^7 $M^{-1}s^{-1}$) indicates that morin is still an efficient quencher of singlet oxygen when it is immobilized on the silica surface. However this value is one order of magnitude lower than that in homogeneous media (1.3×10^8 $M^{-1}s^{-1}$ in D_2O pD 7.4) and erythrocyte ghost membranes dispersed in D_2O pD 7.4 (1.4×10^8 $M^{-1}s^{-1}$)[38]. This could be explained by the interaction between the most acidic hydroxyl moiety of morin (the 2´-OH group on the B ring, pKa 5.2), with the amine group of the NP [53], the formation of dimers and other aggregates of morin on the NP surface, and the slower oxygen diffusion on the solid nanoparticle compared to neat solvents and lipid membranes. In solid organic polymers, the bimolecular quenching rate constants (k_q) for deactivation of singlet oxygen by efficient quenchers are smaller than in homogeneous solutions because quenching process in polymers is mainly controlled by solute diffusion to yield the singlet oxygen-quencher encounter pair [84]. Indeed this reduction in reactivity would be compensated with the higher availability of quencher species, resulting in a potential promissory system for real applications

3.6.2. Reactivity of AMSNPs-MOR against the hydroxyl radical. Consequence of its function as a barrier, the skin is a potential target for oxidative stress due to production of free radicals from different sources. These free radicals threaten the integrity of skin as they do to other tissues [85, 86], but the skin is at risk because its exposition to oxygen from the inside at levels provided by the blood and from the outside at higher levels provided by the air, and the continuous exposition to light [34], which generates hydroxyl radicals through breakage of hydrogen peroxide (H_2O_2 + UV radiation → 2 HO•). Free radicals can also be formed by the

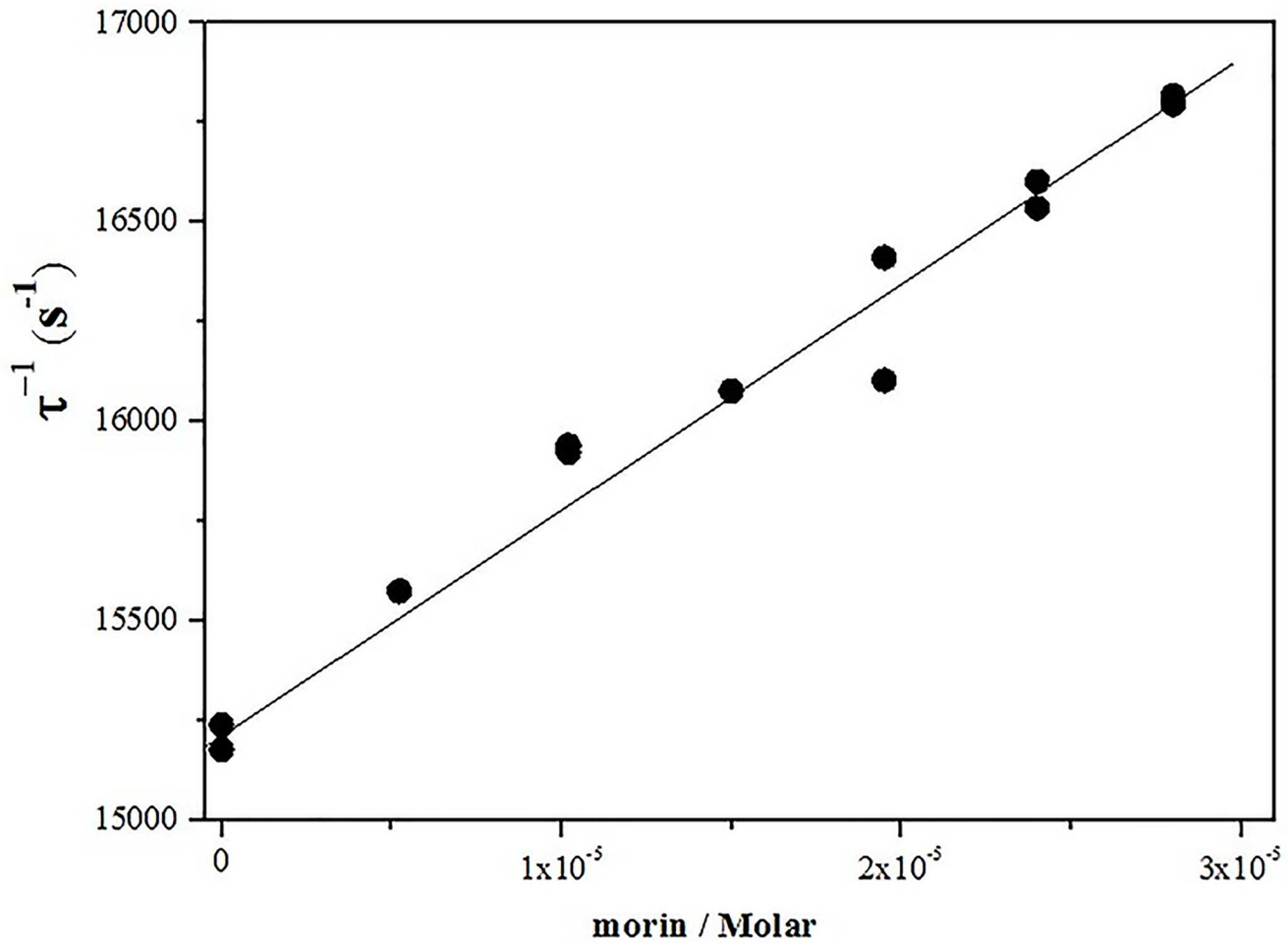

Fig 7. Stern–Volmer type plot for singlet oxygen deactivation by AMSNPs-MOR.

doi:10.1371/journal.pone.0164507.g007

presence of xenobiotics that can contain ions Fe(II) or Cu(I) that act as a catalyst of hydrogen peroxide decomposition (H_2O_2 + Fe(II)/Cu(I) → HO• + HO^- + Fe(III)/Cu(II)).

Morin has shown antioxidant activity against the damage caused by hydroxyl radical, through a proton-coupled electron transfer (PCET mechanism) [87, 88], where the more reactive functional groups in the molecule are the resorcinol moiety in B-ring, or by forming a chelation site for iron ions between 2´-hydroxyl group of ring B and 3-hydroxyl group of ring C [89].

The antioxidant reactivity of AMSNPs-MOR against hydroxyl radical was studied in a system where this radical was generated in situ by hydrogen peroxide 10%v/v UV-photolysis [90, 91]. As described before, morin has been identified as a potent antioxidant against hydroxyl radical [92], but there is no reported information about its antioxidant capacity when absorbed onto silica NPs. The presence of glycerin in the medium generated a hyperfine splitting pattern of six signals that performed a constant intensity in all the spectra, for this reason the analysis became independent of the presence of glycerin (Fig 8A).

To evaluate the scavenging activity of the AMSNPs-MOR, the formation of the DMPO-HO• adduct by every component was measured; the results show that the NP possess scavenging capacity against hydroxyl radical (Fig 8C). On the other hand, the scavenging capacity of

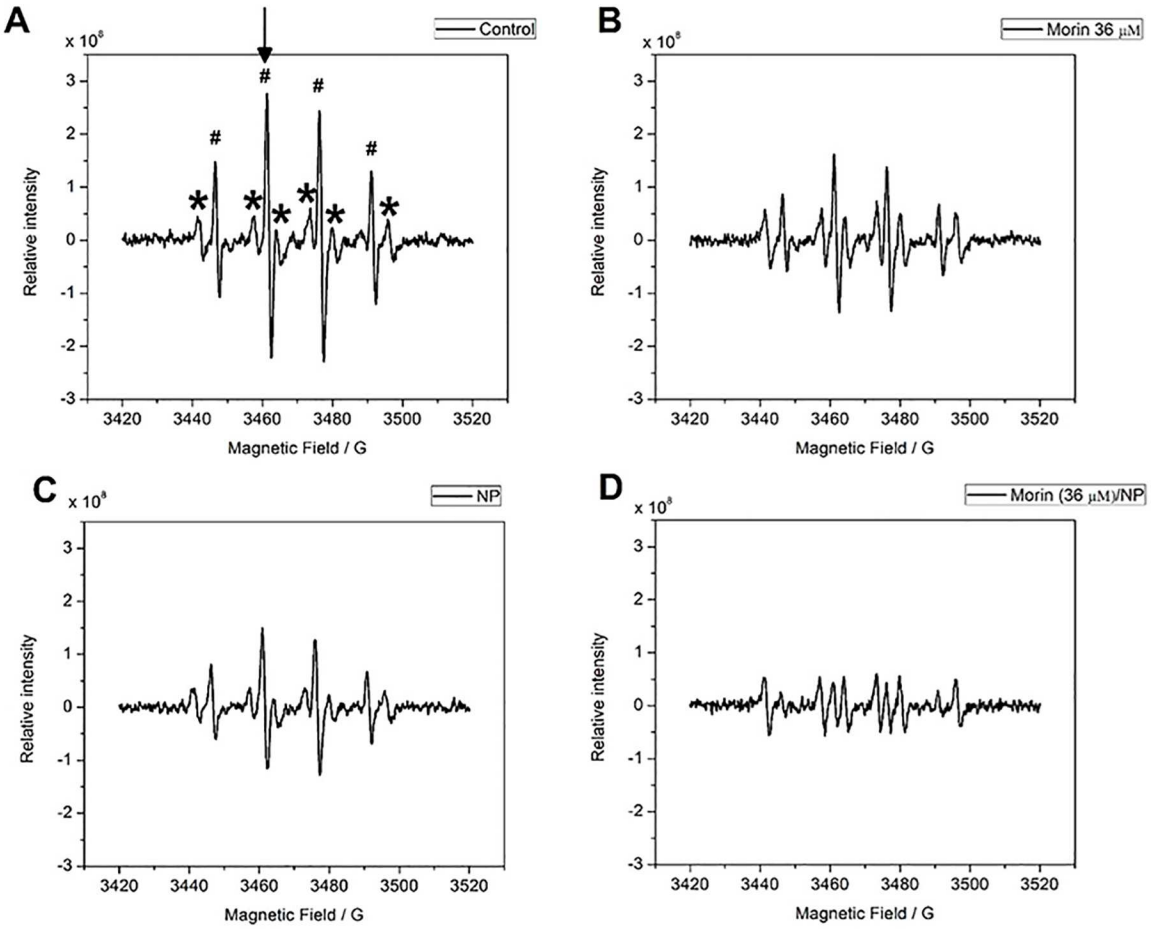

Fig 8. EPR spectra. Control (DMPO + H_2O_2+glycerin 10%); (B) morin (DMPO + H_2O_2 + morin 0.11 mM/glycerin 10%); (C) AMSNPs (DMPO + H_2O_2 + NP 6800 mg L^{-1}/glycerin 10%); (D) AMSNPs-MOR (DMPO + H_2O_2 + morin 0.11 mM/NP 6800 mg L^{-1} /glycerin 10%). In spectrum (A), the symbol **(#)** indicates the presence of DMPO-HO• adduct. The symbol (*) indicates the presence of the DMPO/glycerin adduct; and the arrow indicates the peak that was used for the analysis of each spectrum.

doi:10.1371/journal.pone.0164507.g008

AMSNPs-MOR (Fig 8D) increases in 57% in comparison to morin (at the same concentration) (Fig 8B), which indicates the existence of a synergic effect between the NP and the adsorbed-morin. This synergistic effect has also been observed between SiO_2 nanoparticles and covalently-linked-gallic acid derivative against DPPH• radical [41]. As the antioxidant activity of morin did not decrease when is adsorbed onto the nanoparticles, this may indicate that the resorcinol moiety in B-ring, which is the most reactive site in the molecule against free radicals, is able to interact with hydroxyl radicals. For quercetin, which is structurally similar to morin by replacing the resorcinol in B-ring to a 3',4'-cathecol moiety, when adsorbed onto silica NP, it has been documented a similar behavior against superoxide radical [93], indicating that the B-ring is free to react with the free radicals and that the linkage of this flavonoids to the NP takes place through the polar groups in A and C-rings [59, 94]. The antioxidant capacity against hydroxyl radical is summarized in Fig 9.

4. Conclusions

The aim of this study was to evaluate the antioxidant capacity and the kinetics and the adsorption isotherm of morin onto silica nanoparticles. Mesoporous and spherical aminopropyl-

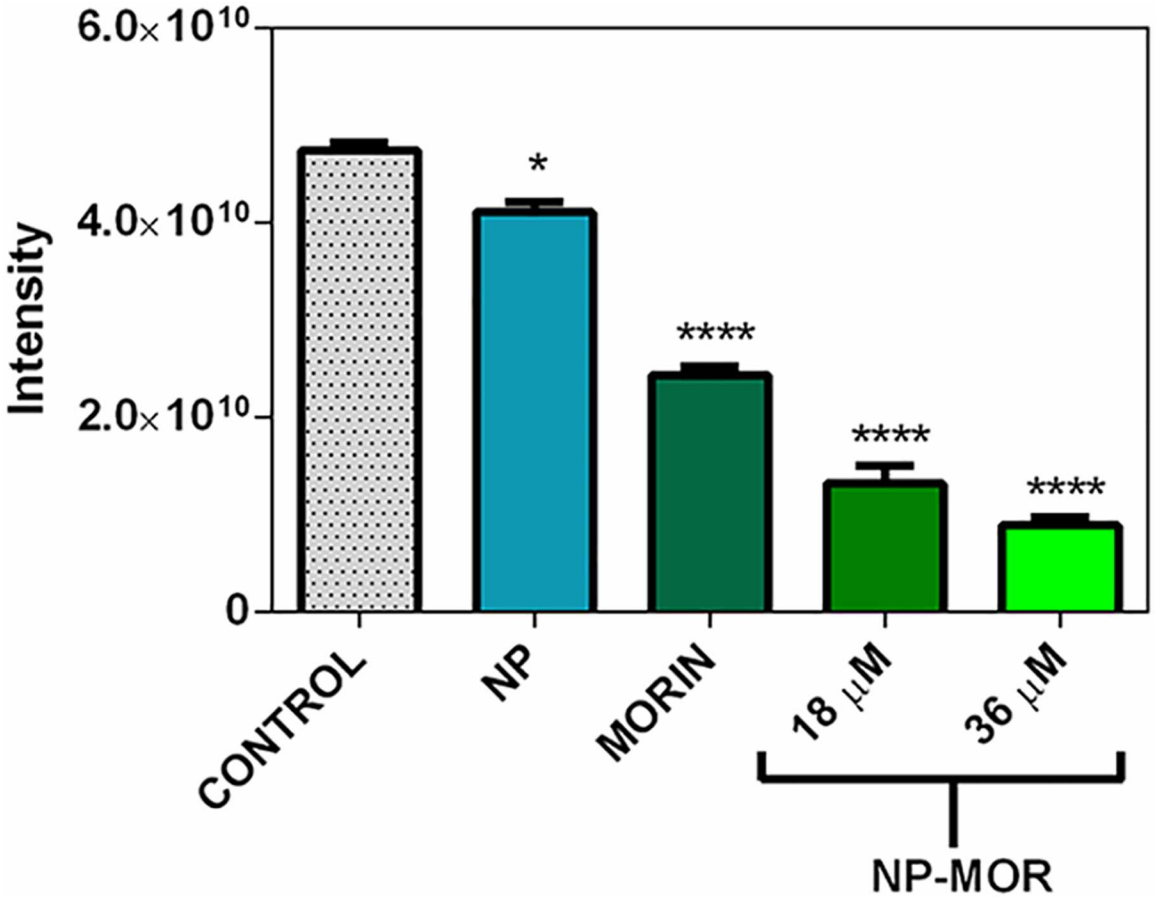

Fig 9. Antioxidant capacity against HO• radical. Control (0 μM morin), AMSNPs (0 μM morin), morin solution suspended in 10% glycerin (MORIN) (36 μM morin), AMSNPs-MOR (18 μM and 36 μM). All the values are given as average ± SD, in three independent assays (*$p < 0.05$ vs. control; ****$p < 0.0001$ vs. control).

doi:10.1371/journal.pone.0164507.g009

modified silica nanoparticles (~150 nm) were prepared and characterized. The maximum adsorption capacity of these nanoparticles for morin (20 mg g^{-1}) was performed by Langmuir, Freundlich and Temkin adsorption isotherms.

The kinetics of morin adsorption onto nanoparticle surface was analyzed using three different kinetic models, the pseudo-first-order proposed first, pseudo-second-order models and intra-particle diffusion model. The results suggest that the process is clearly complex and is more likely that the rate-limiting step of this adsorption system can be a chemisorption rather than an intra-particle diffusion only.

The antioxidant properties of AMSNPs-MOR by monitoring of singlet oxygen deactivation and OH radical scavenging were studied. The total quenching rate constant (k_T) obtained for singlet oxygen deactivation by AMSNPs-MOR was one order of magnitude lower than the morin rate constant reported in homogeneous solvents and lipid membranes. On the other hand, morin behaves as an antioxidant against hydroxyl radical generated *in situ*; nevertheless, NP presented also antioxidant properties by itself. Interestingly, adsorbed morin onto NP exhibits a synergic effect on the antioxidant property against hydroxyl radicals. This effect was increased when increasing the concentration of morin adsorbed, in the concentration range of work.

In summary, taken together the results suggest a complex adsorption process involving at least two ways; first, one monolayer irreversibly adsorbed like bonding-mode and then, presumably, multilayers in a piled up form physisorbed by electrostatic forces. The conjugation, can implicate an interaction between amino group from APTES with carboxyl and/or hydroxyl group on C ring of morin, leading to a resorcinol moiety accessible to react with different ROS or interact with 2′-OH group on the B ring.

Author Contributions

Conceptualization: JM FA OC GG SN FM COA.

Data curation: JM FA FM.

Formal analysis: JM FA OC GG SN FM COA.

Funding acquisition: JM GG COA.

Investigation: JM FA OC GG FM.

Methodology: JM FA OC GG SN FM COA.

Project administration: JM FA.

Resources: JM GG COA.

Supervision: JM FA OC GG SN.

Validation: JM FA GG FM COA.

Visualization: JM FA GG.

Writing – original draft: JM FA OC GG SN FM COA.

Writing – review & editing: JM FA OC GG SN FM COA.

References

1. Elliott J, Hancock B. Pharmaceutical materials science: An active new frontier in materials research. MRS bulletin. 2006; 31:869–73.
2. Peppas NA. Intelligent biomaterials as pharmaceutical carriers in microfabricated and nanoscale devices. MRS bulletin. 2006; 31:888–93.
3. Shah P. Use of nanotechnologies for drug delivery. MRS bulletin. 2006; 31:894–9.
4. Mortera R, Fiorilli S, Garrone E, Verné E, Onida B. Pores occlusion in MCM-41 spheres immersed in SBF and the effect on ibuprofen delivery kinetics: A quantitative model. Chemical Engineering Journal. 2010; 156:184–92.
5. Doane T, Burda C. Nanoparticle mediated non-covalent drug delivery. Adv Drug Deliv Rev. 2013; 65:607–21. doi: 10.1016/j.addr.2012.05.012 PMID: 22664231
6. Ohulchanskyy TY, Roy I, Goswami LN, Chen Y, Bergey EJ, Pandey RK, et al. Organically modified silica nanoparticles with covalently incorporated photosensitizer for photodynamic therapy of cancer. Nano letters. 2007; 7:2835–42. doi: 10.1021/nl0714637 PMID: 17718587
7. Bhaskara Rao BV, Mukherji R, Shitre G, Alam F, Prabhune AA, Kale SN. Controlled release of antimicrobial Cephalexin drug from silica microparticles. Mater Sci Eng C Mater Biol Appl. 2014; 34:9–14. doi: 10.1016/j.msec.2013.10.002 PMID: 24268227
8. Kumar R, Roy I, Ohulchanskyy TY, Goswami LN, Bonoiu AC, Bergey EJ, et al. Covalently dye-linked, surface-controlled, and bioconjugated organically modified silica nanoparticles as targeted probes for optical imaging. Acs Nano. 2008; 2:449–56. doi: 10.1021/nn700370b PMID: 19206569
9. Chen YP, Chen CT, Hung Y, Chou CM, Liu TP, Liang MR, et al. A new strategy for intracellular delivery of enzyme using mesoporous silica nanoparticles: superoxide dismutase. J Am Chem Soc. 2013; 135:1516–23. doi: 10.1021/ja3105208 PMID: 23289802

10. Zhang B, Xing J, Lang Y, Liu H. Synthesis of amino-silane modified magnetic silica adsorbents and application for adsorption of flavonoids from Glycyrrhiza uralensis Fisch. Science in China Series B: Chemistry. 2008; 51:145–51.
11. Sun X, Zhao Y, Lin VS, Slowing, II, Trewyn BG. Luciferase and luciferin co-immobilized mesoporous silica nanoparticle materials for intracellular biocatalysis. J Am Chem Soc. 2011; 133:18554–7. doi: 10.1021/ja2080168 PMID: 22007786
12. Queiroz RG, Varca GHC, Kadlubowski S, Ulanski P, Lugão AB. Radiation-synthesized protein-based drug carriers: Size-controlled BSA nanoparticles. International Journal of Biological Macromolecules. 2016; 85:82–91. doi: 10.1016/j.ijbiomac.2015.12.074 PMID: 26730485
13. Kupetz E, Bunjes H. Lipid nanoparticles: drug localization is substance-specific and achievable load depends on the size and physical state of the particles. J Control Release. 2014; 189:54–64. doi: 10.1016/j.jconrel.2014.06.007 PMID: 24933601
14. Mehnert W, Mäder K. Solid lipid nanoparticles. Adv Drug Deliv Rev. 2012; 64:83–101.
15. Masood F. Polymeric nanoparticles for targeted drug delivery system for cancer therapy. Mater Sci Eng C Mater Biol Appl. 2016; 60:569–78. doi: 10.1016/j.msec.2015.11.067 PMID: 26706565
16. Yue H, Ma G. Polymeric micro/nanoparticles: Particle design and potential vaccine delivery applications. Vaccine. 2015; 33:5927–36. doi: 10.1016/j.vaccine.2015.07.100 PMID: 26263197
17. Chandran PR, Thomas RT. Gold Nanoparticles in Cancer Drug Delivery. 2015:221–37.
18. Rai M, Ingle AP, Gupta I, Brandelli A. Bioactivity of noble metal nanoparticles decorated with biopolymers and their application in drug delivery. Int J Pharm. 2015; 496:159–72. doi: 10.1016/j.ijpharm.2015.10.059 PMID: 26520406
19. Wang Y, Zhao Q, Han N, Bai L, Li J, Liu J, et al. Mesoporous silica nanoparticles in drug delivery and biomedical applications. Nanomedicine. 2015; 11:313–27. doi: 10.1016/j.nano.2014.09.014 PMID: 25461284
20. Liberman A, Mendez N, Trogler WC, Kummel AC. Synthesis and surface functionalization of silica nanoparticles for nanomedicine. Surf Sci Rep. 2014; 69:132–58. doi: 10.1016/j.surfrep.2014.07.001 PMID: 25364083
21. Tang L, Cheng J. Nonporous Silica Nanoparticles for Nanomedicine Application. Nano Today. 2013; 8:290–312. doi: 10.1016/j.nantod.2013.04.007 PMID: 23997809
22. Park JT, Seo JA, Ahn SH, Kim JH, Kang SW. Surface modification of silica nanoparticles with hydrophilic polymers. Journal of Industrial and Engineering Chemistry. 2010; 16:517–22.
23. Qiao B, Liang Y, Wang T-J, Jiang Y. Surface modification to produce hydrophobic nano-silica particles using sodium dodecyl sulfate as a modifier. Applied Surface Science. 2015.
24. Wang X, Wang P, Jiang Y, Su Q, Zheng J. Facile surface modification of silica nanoparticles with a combination of noncovalent and covalent methods for composites application. Composites Science and Technology. 2014; 104:1–8.
25. Guo Y, Rogelj S, Zhang P. Rose Bengal-decorated silica nanoparticles as photosensitizers for inactivation of gram-positive bacteria. Nanotechnology. 2010; 21:065102. doi: 10.1088/0957-4484/21/6/065102 PMID: 20061596
26. Uppal A, Jain B, Gupta PK, Das K. Photodynamic action of Rose Bengal silica nanoparticle complex on breast and oral cancer cell lines. Photochem Photobiol. 2011; 87:1146–51. doi: 10.1111/j.1751-1097.2011.00967.x PMID: 21749397
27. Venu Gopal J. Morin Hydrate: Botanical origin, pharmacological activity and its applications: A mini-review. Pharmacognosy Journal. 2013; 5:123–6.
28. Sivaramakrishnan V, Devaraj SN. Morin fosters apoptosis in experimental hepatocellular carcinogenesis model. Chem Biol Interact. 2010; 183:284–92. doi: 10.1016/j.cbi.2009.11.011 PMID: 19931519
29. Iglesias CV, Aparicio R, Rodrigues-Simioni L, Camargo EA, Antunes E, Marangoni S, et al. Effects of morin on snake venom phospholipase A2 (PLA2). Toxicon. 2005; 46:751–8. doi: 10.1016/j.toxicon.2005.07.017 PMID: 16185736
30. Govindasamy C, Alnumair KS, Alsaif MA. GW25-e5392 Morin, a flavonoid, on lipid peroxidation and antioxidant status in experimental myocardial ischemic rats. Journal of the American College of Cardiology. 2014; 64:C56.
31. Prahalathan P, Kumar S, Raja B. Morin attenuates blood pressure and oxidative stress in deoxycorticosterone acetate-salt hypertensive rats: a biochemical and histopathological evaluation. Metabolism. 2012; 61:1087–99. doi: 10.1016/j.metabol.2011.12.012 PMID: 22386933
32. Wu T-W, Fung K-P, Zeng L-H, Wu J, Hempel A, Grey AA, et al. Molecular properties and myocardial salvage effects of morin hydrate. Biochemical pharmacology. 1995; 49:537–43. PMID: 7872959

33. Lee J, Shin YK, Song JY, Lee KW. Protective mechanism of morin against ultraviolet B-induced cellular senescence in human keratinocyte stem cells. Int J Radiat Biol. 2014; 90:20–8. doi: 10.3109/09553002.2013.835502 PMID: 23952478

34. Shetty PK, Venuvanka V, Jagani HV, Chethan GH, Ligade VS, Musmade PB, et al. Development and evaluation of sunscreen creams containing morin-encapsulated nanoparticles for enhanced UV radiation protection and antioxidant activity. Int J Nanomedicine. 2015; 10:6477–91. doi: 10.2147/IJN.S90964 PMID: 26508854

35. Parisi OI, Puoci F, Restuccia D, Farina G, Iemma F, Picci N. Polyphenols and Their Formulations. 2014:29–45.

36. Markovic Z, Milenkovic D, Dorovic J, Dimitric Markovic JM, Stepanic V, Lucic B, et al. Free radical scavenging activity of morin 2'-O(-) phenoxide anion. Food Chem. 2012; 135:2070–7. doi: 10.1016/j.foodchem.2012.05.119 PMID: 22953958

37. Zhang R, Kang KA, Piao MJ, Maeng YH, Lee KH, Chang WY, et al. Cellular protection of morin against the oxidative stress induced by hydrogen peroxide. Chem Biol Interact. 2009; 177:21–7. doi: 10.1016/j.cbi.2008.08.009 PMID: 18793623

38. Gunther G, Berrios E, Pizarro N, Valdes K, Montero G, Arriagada F, et al. Flavonoids in Microheterogeneous Media, Relationship between Their Relative Location and Their Reactivity towards Singlet Oxygen. PLoS One. 2015; 10:e0129749. doi: 10.1371/journal.pone.0129749 PMID: 26098745

39. Morales J, Gunther G, Zanocco AL, Lemp E. Singlet oxygen reactions with flavonoids. A theoretical-experimental study. PLoS One. 2012; 7.

40. Nagai S, Ohara K, Mukai K. Kinetic study of the quenching reaction of singlet oxygen by flavonoids in ethanol solution. The Journal of Physical Chemistry B. 2005; 109:4234–40. doi: 10.1021/jp0451389 PMID: 16851486

41. Deligiannakis Y, Sotiriou GA, Pratsinis SE. Antioxidant and antiradical SiO_2 nanoparticles covalently functionalized with gallic acid. ACS Appl Mater Interfaces. 2012; 4:6609–17. doi: 10.1021/am301751s PMID: 23121088

42. Schlipf DM, Jones CA, Armbruster ME, Rushing ES, Wooten KC, Rankin SE, et al. Flavonoid adsorption and stability on titania-functionalized silica nanoparticles. Colloids and Surfaces A: Physicochemical and Engineering Aspects. 2015; 478:15–21.

43. Stöber W, Fink A, Bohn E. Controlled growth of monodisperse silica spheres in the micron size range. J Colloid Interface Sci. 1968; 26:62–9.

44. Limousin G, Gaudet JP, Charlet L, Szenknect S, Barthès V, Krimissa M. Sorption isotherms: A review on physical bases, modeling and measurement. Applied Geochemistry. 2007; 22:249–75.

45. Sposito G. The chemistry of soils: Oxford university press; 2008.

46. Morales J, Zanocco A, Günther G, Lemp E. A high-performance liquid chromatography method for determination of flavonoids in dipalmitoylphosphatidilcholine liposome solutions. Afinidad. 2009; 539: 56–61.

47. Tien C, Ramarao BV. Further examination of the relationship between the Langmuir kinetics and the Lagergren and the second-order rate models of batch adsorption. Separation and Purification Technology. 2014; 136:303–8.

48. Mura F, Silva T, Castro C, Borges F, Zuniga MC, Morales J, et al. New insights into the antioxidant activity of hydroxycinnamic and hydroxybenzoic systems: spectroscopic, electrochemistry, and cellular studies. Free Radic Res. 2014; 48:1473–84 doi: 10.3109/10715762.2014.965702 PMID: 25236566

49. Endo N, Oowada S, Sueishi Y, Shimmei M, Makino K, Fujii H, et al. Serum hydroxyl radical scavenging capacity as quantified with iron-free hydroxyl radical source. Journal of clinical biochemistry and nutrition. 2009; 45:193. doi: 10.3164/jcbn.08-265 PMID: 19794928

50. Zeleňák V, Badaničová M, Halamová D, Čejka J, Zukal A, Murafa N, Goerigk G. Amine-modified ordered mesoporous silica: Effect of pore size on carbon dioxide capture. Chemical Engineering Journal. 2008; 144: 336–342.

51. Zhou H, Sun J, Wu X, Ren B, Wang J. Tailored morphology and controlled structure of bimodal mesopores silicas via additive ammonia amount in the TEOS-CTAB-H2O system. Materials Chemistry and Physics. 2013; 140: 148–153.

52. Yue Pu Y, Li Y, Zhuang W, Zhang M, Zong Li B, Gang Yang Y. Preparation and characterizations of helical mesoporous silica nanorods using CTAB and alcohols. Chinese Chemical Letters. 2012; 23: 1201–1204.

53. Musialik M, Kuzmicz R, Pawłowski TS, Litwinienko G. Acidity of hydroxyl groups: an overlooked influence on antiradical properties of flavonoids. The Journal of organic chemistry. 2009; 74:2699–709. doi: 10.1021/jo802716v PMID: 19275193

54. Beganskienė A, Sirutkaitis V, Kurtinaitienė M, Juškėnas R, Kareiva A. FTIR, TEM and NMR investigations of Stöber silica nanoparticles. Mater Sci (Medžiagotyra). 2004; 10:287–90.

55. Kamiya H, Mitsui M, Takano H, Miyazawa S. Influence of Particle Diameter on Surface Silanol Structure, Hydration Forces, and Aggregation Behavior of Alkoxide-Derived Silica Particles. Journal of the American Ceramic Society. 2000; 83:287–93.

56. Pasternack RM, Rivillon Amy S, Chabal YJ. Attachment of 3-(aminopropyl) triethoxysilane on silicon oxide surfaces: dependence on solution temperature. Langmuir. 2008; 24:12963–71. doi: 10.1021/la8024827 PMID: 18942864

57. Pena-Alonso R, Rubio F, Rubio J, Oteo J. Study of the hydrolysis and condensation of γ-Aminopropyltriethoxysilane by FT-IR spectroscopy. Journal of materials science. 2007; 42:595–603.

58. Rahman I, Jafarzadeh M, Sipaut C. Synthesis of organo-functionalized nanosilica via a co-condensation modification using γ-aminopropyltriethoxysilane (APTES). Ceramics International. 2009; 35:1883–8.

59. Vergara-Castañeda H, Hernandez-Martinez AR, Estevez M, Mendoza S, Luna-Barcenas G, Pool H. Quercetin conjugated silica particles as novel biofunctional hybrid materials for biological applications. J Colloid Interface Sci. 2016; 466:44–55. doi: 10.1016/j.jcis.2015.12.011 PMID: 26704475

60. Gao ZP, Yu ZF, Yue TL, Quek SY. Adsorption isotherm, thermodynamics and kinetics studies of polyphenols separation from kiwifruit juice using adsorbent resin. Journal of Food Engineering. 2013; 116:195–201.

61. Azizian S. Kinetic models of sorption: a theoretical analysis. J Colloid Interface Sci. 2004; 276:47–52. doi: 10.1016/j.jcis.2004.03.048 PMID: 15219428

62. Berlier G, Gastaldi L, Sapino S, Miletto I, Bottinelli E, Chirio D, et al. MCM-41 as a useful vector for rutin topical formulations: synthesis, characterization and testing. International journal of pharmaceutics. 2013; 457:177–86. doi: 10.1016/j.ijpharm.2013.09.018 PMID: 24076399

63. Bhattacharya K, Parasar D, Mondal B, Deb P. Mesoporous magnetic secondary nanostructures as versatile adsorbent for efficient scavenging of heavy metals. Sci Rep. 2015; 5:17072. doi: 10.1038/srep17072 PMID: 26602613

64. Langmuir I. The constitution and fundamental properties of solids and liquids. Part I. Solids. Journal of the American Chemical Society. 1916; 38:2221–95.

65. Langmuir I. The constitution and fundamental properties of solids and liquids. II. Liquids. 1. Journal of the American Chemical Society. 1917; 39:1848–906.

66. Foo KY, Hameed BH. Insights into the modeling of adsorption isotherm systems. Chemical Engineering Journal. 2010; 156:2–10.

67. Eriksson M, Lundström I, Ekedahl L-G. A model of the Temkin isotherm behavior for hydrogen adsorption at Pd–SiO_2 interfaces. Journal of applied physics. 1997; 82:3143–6.

68. Liu W, Guo R. The interaction between morin and CTAB aggregates. J Colloid Interface Sci. 2005; 290:564–73. doi: 10.1016/j.jcis.2005.04.061 PMID: 16009368

69. Ho Y-S, Ofomaja AE. Kinetics and thermodynamics of lead ion sorption on palm kernel fibre from aqueous solution. Process Biochemistry. 2005; 40:3455–61.

70. Hall KR, Eagleton LC, Acrivos A, Vermeulen T. Pore-and solid-diffusion kinetics in fixed-bed adsorption under constant-pattern conditions. Industrial & Engineering Chemistry Fundamentals. 1966; 5:212–23.

71. Ghaedi M, Ansari A, Habibi MH, Asghari AR. Removal of malachite green from aqueous solution by zinc oxide nanoparticle loaded on activated carbon: Kinetics and isotherm study. Journal of Industrial and Engineering Chemistry. 2014; 20:17–28.

72. Qiu H, Lv L, Pan B-c, Zhang Q-j, Zhang W-m, Zhang Q-x. Critical review in adsorption kinetic models. Journal of Zhejiang University Science A. 2009; 10:716–24.

73. Boyd G, Adamson A, Myers L Jr. The exchange adsorption of ions from aqueous solutions by organic zeolites. II. Kinetics1. Journal of the American Chemical Society. 1947; 69:2836–48. PMID: 20270838

74. Liu Y, Liu Y-J. Biosorption isotherms, kinetics and thermodynamics. Separation and Purification Technology. 2008; 61:229–42.

75. Tseng R-L, Wu F-C, Juang R-S. Characteristics and applications of the Lagergren's first-order equation for adsorption kinetics. Journal of the Taiwan Institute of Chemical Engineers. 2010; 41:661–9.

76. Ho Y-S, McKay G. Sorption of dye from aqueous solution by peat. Chemical Engineering Journal. 1998; 70:115–24.

77. Chen Y, Zhang D. Adsorption kinetics, isotherm and thermodynamics studies of flavones from Vaccinium Bracteatum Thunb leaves on NKA-2 resin. Chemical Engineering Journal. 2014; 254:579–85.

78. Vasiliu S, Bunia I, Racovita S, Neagu V. Adsorption of cefotaxime sodium salt on polymer coated ion exchange resin microparticles: Kinetics, equilibrium and thermodynamic studies. Carbohydrate Polymers. 2011; 85:376–87.

79. Anbia M, Hariri SA. Removal of methylene blue from aqueous solution using nanoporous SBA-3. Desalination. 2010; 261:61–6.

80. Anbia M, Hariri SA, Ashrafizadeh SN. Adsorptive removal of anionic dyes by modified nanoporous silica SBA-3. Applied Surface Science. 2010; 256:3228–33.

81. Anbia M, Salehi S. Removal of acid dyes from aqueous media by adsorption onto amino-functionalized nanoporous silica SBA-3. Dyes and Pigments. 2012; 94:1–9.

82. Devasagayam TP, Kamat JP. Biological significance of singlet oxygen. Indian journal of experimental biology. 2002; 40:680–92. PMID: 12587716

83. Berneburg M, Grether-Beck S, Kürten V, Ruzicka T, Briviba K, Sies H, et al. Singlet oxygen mediates the UVA-induced generation of the photoaging-associated mitochondrial common deletion. Journal of Biological Chemistry. 1999; 274:15345–9. PMID: 10336420

84. Ogilby PR, Dillon MP, Kristiansen M, Clough RL. Quenching of singlet oxygen in solid organic polymers. Macromolecules. 1992; 25:3399–405.

85. Bickers DR, Athar M. Oxidative stress in the pathogenesis of skin disease. Journal of Investigative Dermatology. 2006; 126:2565–75. doi: 10.1038/sj.jid.5700340 PMID: 17108903

86. Darr D, Fridovich I. Free radicals in cutaneous biology. Journal of Investigative Dermatology. 1994; 102:671–5. PMID: 8176246

87. Amić A, Marković Z, Marković JMD, Stepanić V, Lučić B, Amić D. Towards an improved prediction of the free radical scavenging potency of flavonoids: The significance of double PCET mechanisms. Food Chem. 2014; 152:578–85. doi: 10.1016/j.foodchem.2013.12.025 PMID: 24444978

88. Liu W, Guo R. Effects of Triton X-100 nanoaggregates on dimerization and antioxidant activity of morin. Molecular pharmaceutics. 2008; 5:588–97. doi: 10.1021/mp7001413 PMID: 18510337

89. Mladěnka P, Macáková K, Filipský T, Zatloukalová L, Jahodář L, Bovicelli P, et al. In vitro analysis of iron chelating activity of flavonoids. Journal of inorganic biochemistry. 2011; 105:693–701. doi: 10.1016/j.jinorgbio.2011.02.003 PMID: 21450273

90. Finkelstein E, Rosen GM, Rauckman EJ. Spin trapping. Kinetics of the reaction of superoxide and hydroxyl radicals with nitrones. Journal of the American Chemical Society. 1980; 102:4994–9.

91. Goldstein S, Aschengrau D, Diamant Y, Rabani J. Photolysis of aqueous H2O2: quantum yield and applications for polychromatic UV actinometry in photoreactors. Environmental science & technology. 2007; 41:7486–90.

92. Husain SR, Cillard J, Cillard P. Hydroxyl radical scavenging activity of flavonoids. Phytochemistry. 1987; 26:2489–91.

93. Lee GH, Lee SJ, Jeong SW, Kim H-C, Park GY, Lee SG, et al. Antioxidative and antiinflammatory activities of quercetin-loaded silica nanoparticles. Colloids and Surfaces B: Biointerfaces. 2016.

94. Zhou Q, Zhang H, Wang Y, Zhou X. Studies on the interaction of interface between morin and TiO2. Spectrochimica Acta Part A: Molecular and Biomolecular Spectroscopy. 2009; 72:110–4.